

RESEARCH

Open Access



Channel state information-based wireless localization by signal reconstruction

Yunbing Hu^{1,3}, Ao Peng^{1*†}, Shenghong Li^{2†}, Biyu Tang^{1†}, Wei Ni^{2†}, Xianzhi Lu^{3†} and Jianguo Tang^{3†}

[†]Ao Peng, Shenghong Li, Biyu Tang, Wei Ni, Xianzhi Lu, Jianguo Tang contributed equally to this work.

*Correspondence: pa@xmu.edu.cn

¹School of Informatics, Xiamen University, Xiamen 361001, Fujian, China

²Commonwealth Scientific and Industrial Research Organisation (CSIRO), Marsfield, Sydney, NSW 2122, Australia

³Chongqing College of Electronic Engineering, Chongqing 401331, China

Abstract

Wireless localization technology has been widely used in indoor and outdoor fields. Channel estimation based on channel state information is a hot research topic in recent years. However, due to the interference of acquisition bandwidth, noise and Doppler effect, high-resolution channel estimation is a difficult problem. In this paper, the least squares estimate the amplitude of the signal subspace projection and estimate the time delay, using wireless channel state information to delay obey exponential distribution and magnitude obey normal distribution features, and reconstruction after the signal space and sampling to the Euclidean distance between the signal space, common as gradient optimization parameters, estimate the arrival time delay of high precision. The algorithm proposed in this paper filters out the noise interference in wireless communication and improves the accuracy of channel estimation through the method of least square and gradient optimization, which provides a feasible scheme for indoor wireless localization.

Keywords: Channel state information, Channel estimation, Subspace projection, Gradient descent methods

1 Introduction

The huge market demand for wireless localization-based services has aroused great research interest [1, 2]. Satellite signals do not perform effectively in airports, prisons, hospitals, warehouses, shopping, valleys, etc. Therefore, other wireless positioning services are needed to supplement satellite positioning.

At present, in addition to the satellite positioning technology, there are positioning technologies such as bluetooth [3, 4], radar [5], radio frequency identification (RFID) [6], ultra-wideband (UWB) [7], geomagnetic field [8], visible light [9], thermal infrared [10] and sound [11]. Most of these positioning technologies, however, require additional hardware anchor points, increasing business costs. The ubiquitous WiFi [12–14] radio signal provides broader convenience for the promotion and use of a business.

In recent years, there have been two kinds of signals collected in the methods based on WiFi localization. One is the technology based on the received signal strength indicator (RSSI) of radio signals [15–20], and the other is the CSI-based [21] technology that reflects the state of the radio signal. RSSI is sensitive to time-varying multipath fading, and RSSI is obtained by power integration in the digital domain and

then backward pushing to the antenna port. The inconsistent transmission characteristics of reverse channel signals and the sensitivity to multipath fading will affect the positioning accuracy of RSSI. CSI describes signal decay factors along each transmission path, providing phases and amplitudes of multiple sub-carriers, i.e., signal scattering, environmental fading, etc. Information, such as multipath fading or shadowing fading and power decay of distance, is accurate information about the environment while signals are being relayed. Therefore, it is possible to achieve more accurate positioning through CSI. However, due to interference signals and different positioning scenes, it is difficult to estimate the TOA used for positioning by CSI accurately.

Recently, there are three main methods based on CSI localization research: one is based on fingerprint localization method, the second is based on data fusion localization method, and the other is based on geometry localization method. Fingerprint-based localization method needs to collect real-time data in advance. ILCL proposed by Zhu et al. [22] is an intelligent positioning scheme based on incremental learning without retraining model, in a 200 square meter location scene, and the average accuracy of the location of the conference room average positioning error is 1.39968 m. Wei et al. [23] used a regression formula to train the positioning accuracy of convolutional neural networks (CNNs) to reach about 50% within the range of 1 m. CiFi proposed by Wang et al. [24] achieves the mean distance error reaches the lowest value of 2.3863 m in the corridor experiment. Chen et al. [25] adopted a convolutional neural network (CNN) to localization in a room, which performs the best with results in maximal localization error of 0.92 m with a probability of 99.97%. Jing et al. [26] proposed a fingerprinting localization system based on a dual-stream three-dimensional convolutional neural network (DS-3DCNN) in a room, and the mean distance error reaches the lowest value of 0.984 m in the laboratory environment. In [27], a multi-view discriminant learning approach was developed for indoor localization that exploits both the amplitude and the phase information of CSI to create feature images for each location, and the minimum distance errors for the laboratory and corridor experiments are 0.205 m and 0.109 m, respectively. Y. -W. he combines unsupervised learning with supervised learning in neural network (NN) model for indoor location based on channel state information (CSI). In the case of a bandwidth of 20 MHz, the error is about 50% within 1 m. In [21], the authors proposed to transform the measured data of CSI into images and use the classification ability of CNN for localization, and 70% of the test cases have a localization error under 1.5 ms.

It can be seen from the above paper that the fingerprint-based positioning method has the advantage of high positioning accuracy. Still, it needs to pre-sample the field data to build the positioning model. Once the location of the positioning reference node changes, it needs to re-collect the field data and update the positioning system, which brings inconvenience to commercial applications.

Zhao et al. [28] proposed a data fusion method of fingerprinting using RSS and CSI data from single access points, which can achieve a positioning accuracy of 1.79 ms in a typical laboratory. Li et al. [29] proposed an enhanced particle filter based positioning method that combines CSI information and inertial sensor information to achieve an average accuracy of 1.3m. A data fusion-based positioning method can obtain

higher positioning accuracy, but it needs more data sources, which is not very favorable for commercial promotion.

In [30], Manikanta et al. used multiple measurement angle-of-arrival (AoA) to achieve positioning on standard WiFi equipment, and 60% of localization error reaches about 1-meter indoor office deployment. In [31], WiFi devices were located by using the round-trip delay (RTD) and AOA measurements, which requires changes to the firmware of target devices. The MUSIC algorithm proposed by Schmidt et al. [32] has a good effect in terms of resolution, estimation accuracy and stability under the condition of multiple antennas. ArrayTrack [33] proposed by Jie et al. is similar to [32], requiring eight antennas. However, the number of antennas of commercial WiFi devices is generally small, and it is difficult to use the multi-antenna method for positioning in application and promotion. Finding a suitable commercial application promotion and better positioning effect positioning method urgently needs to solve the problem.

This paper proposes a CSI-based localization algorithm that locates standard WiFi devices, achieving higher accuracy than existing approaches based on the celebrated MUSIC and ESPRIT algorithms, with low communication and computational cost in applications. The main contributions of this work are as follows:

1. An efficient algorithm based on subspace projection is proposed for ToA estimation, providing coarse TOA measurements with low computational complexity.
2. An accurate ToA estimation algorithm is proposed, which refines the coarse ToA measurement through CSI reconstruction and achieves higher accuracy than existing MUSIC and ESPRIT-based algorithms.
3. Experimental verification is carried out on an outdoor positioning system with six anchor points which were used in 900 m² of outdoor measurement. The results show that the proposed algorithm has high precision and broad application prospects.

The proposed algorithm can effectively reduce the cost of commercial deployment and improve the versatility of the equipment because it does not need to collect the data of the localization area in advance. The positioning error is reduced to 0.75 m in 80% and 1 m in 90% in an outdoor environment. In the indoor positioning environment, the positioning errors of the algorithm are reduced to 0.75 m and 1 m in the range of 60% and 74%, respectively.

The remainder of this paper is organized as follows. The system model, including system architecture and signal structure, is presented in Sect. 2. The problem-solving process is presented in Sect. 3. We present the process of solving TOA by the signal reconstruction proposed. Experimental validation is provided in Sect. 4, followed by concluding remarks in Sect. 5.

2 System model

In the section, we briefly introduce the positioning equipment and system structure, then introduce the source and data structure of the positioning data, and finally present the Saleh-Valenzuela propagation model.

2.1 System architecture

In this paper, we use the WiFi-based wireless ad hoc system for positioning (WiFi-WASP) [34–36] developed by the Commonwealth Scientific and Industrial Research Organization (CSIRO) of Australia for our experiments. The WiFi-WASP platform is a software-defined radio built with low-cost off-the-shelf hardware, which operates in the 5.8 GHz ISM band.

Figure 1 shows the structure of the time-difference-of-arrival (TDOA)-based passive WiFi localization system. The localization system consists of six custom-built WiFi sniffers that act as anchors for deployment at known locations, a target device for localization, an access point (AP) for WiFi communication and a computer. Ordinary WiFi access points can replace sniffers with a sniffing function. Not only can the sniffer be used to monitor the traffic in the WiFi network [37], but also has the ability to sniff the communication between the target device and WiFi. More importantly, it will not interfere with the operation of existing standard WiFi systems. The clock skew and clock offset of the system clock is estimated by the timestamps of the access point communication measured by all the sniffers [38], which solves the clock synchronization problem by using the time-of-arrival (TOA). The target device used for positioning is located in the standard WiFi wireless network. When the target device communicates with the AP, all the sniffer measurements will measure the communication time stamp. At the same time, combined with the AP communication time stamp measured by the sniffer, the location of the target device can be estimated on the computer.

2.2 Signal structure

802.11a/g/n/ac WiFi devices adopt the OFDM modulation scheme [39, 40]. Figure 2 illustrates the architecture of a WiFi system. On the transmitter side, the transmitted symbols that need to be transmitted are encoded, the serial-to-parallel data stream is converted, and then the signal is converted from the frequency domain to the time domain using the inverse Fourier transform. To reduce inter-symbol interference, circular prefixes (CP) are inserted to form OFDM codes. When framing, the

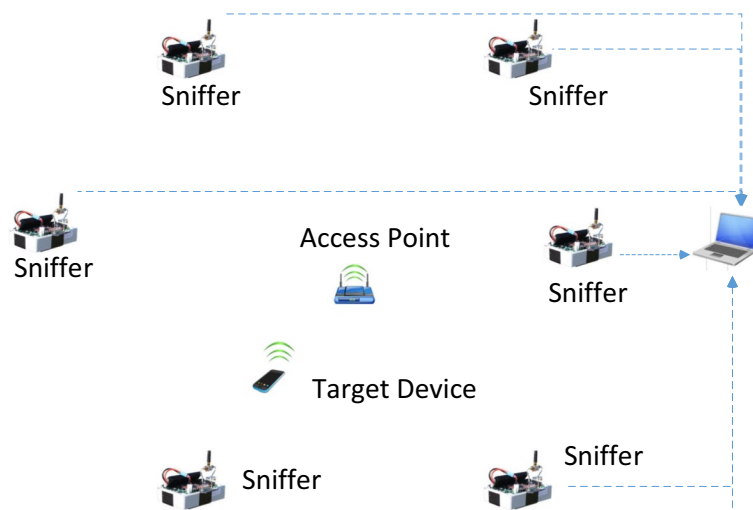


Fig. 1 Structure of the time-difference-of-arrival (TDOA)-based passive WiFi localization system

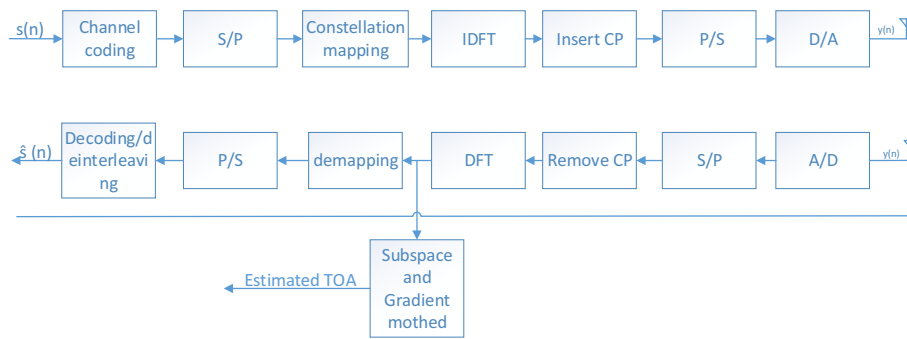


Fig. 2 Point-to-point transmission of model using OFDM

synchronization sequence and channel estimation sequence must be added to facilitate the burst detection, synchronization and channel estimation of the receiver, and finally output the orthogonal baseband signal. The reception of OFDM is the inverse of the transmission process, which is used to recover the data at the receiver. However, CSI for TOA estimation is the frequency-domain data after the signal has passed through the discrete Fourier transform (DFT), the instantaneous CSI measured by the receiver, in Fig. 2. The CSI is extracted without any computing overhead and provides a wealth of fine-grain information, such as dye out, multipath fading or shadowing fading, power decay of distance and noise.

The WiFi-WASP devices platform implements a traditional OFDM receiver, along with a sub-system that estimates the ToA of each received frame from channel state information using the proposed subspace projection and gradient descent method. In order to improve the positioning accuracy, the instantaneous automatic gain control data of the sensor is also extracted to compensate the signal delay [41, 42].

The CSI data collected by the WiFi-WASP system is processed on PC for TOA estimation. Specifically, the CSI associated with each received WiFi frame can be expressed as:

$$\mathbf{H} = [\mathbf{h}_1, \mathbf{h}_2, \dots, \mathbf{h}_i]^T, i \in [1, \infty), \tag{1}$$

where \mathbf{H} collects all CSI values between the sniffer and the AP and between the target device measured by the sniffer and the AP. \mathbf{h}_i is the *i*th the TOA signal sampled from the WASP. \mathbf{H} is defined in the frequency domain as [43]:

$$H_{ij} = \|H_{ij}\|e^{j\angle H_{ij}}, j \in [1, 256], \tag{2}$$

where H_{ij} is the *i*th sub-carriers of CSI, amplitude $\|H_{ij}\|$, and phase $\angle H_{ij}$, show signal attenuation and phase shift, and *j* indicates that each CSI group has 256 complex numbers.

The CSI is fine-grained information from the physical layer that describes channel frequency response (CFR) from the transmitter to the receiver. However, to estimate the TOA used for positioning, channel impulse response (CIR), which can describe the multipath effect, is needed to represent the channel. In the case of infinite bandwidth, CFR and CIR are converted to each other by Fourier transforms. Therefore, the received CSI data, under the assumption of linear time invariance, CIR can be expressed as:

$$h(\tau) = \sum_{k=0}^{L-1} \alpha_k \delta(\tau - \tau_k), k \in [1, 256], \tag{3}$$

where a_k and τ_k denote the amplitude of the multipath component and the complex attenuation and propagation delay of the k th path, respectively. $\delta(\tau)$ is the Dirac delta function, and L is the number of multipath components, while $1 \leq k \leq L$ are in ascending order. L is related to the sampling points that CFR converts into CIR by Fourier transform, and 256 sampling points are used in this paper. So, τ_0 in the model denotes the propagation delay the direct line-of-sight path, which is the TOA used to calculate the location. CIR shows the signal energy value of the signal reaches the receiver at different times.

2.3 Channel modeling

In order to reconstruct the signal space in the frequency domain, the Saleh-Valenzuela propagation model (SVPM) and Monte Carlo simulation were used to obtain the characteristics of amplitude and propagation delay [44, 45]. Figure 3 shows three clusters, each containing four paths. In the SVPM channel model, the two-stage Poisson process is used to simulate the arrival of the multipath cluster and the multipath component within the cluster received by the receiver. The TOAs of both are independent and identically distributed exponential distribution, so the complex amplitude of each path can be expressed as [44, 45]:

$$a_k = N(0, \sigma_k^2) + jN(0, \sigma_k^2), \tag{4}$$

where k indicates the number of path, and $N(0, \sigma_k^2)$ shows a value which is according with the normal distribution. (4) creates the Rayleigh fading. The variance σ_k^2 is the average power of the k path, so the strength of the paths within the clusters is given as [44, 45]:

$$\sigma^2(k) = e^{-T_l/\Gamma} e^{-\tau_{il}/\gamma}, \tag{5}$$

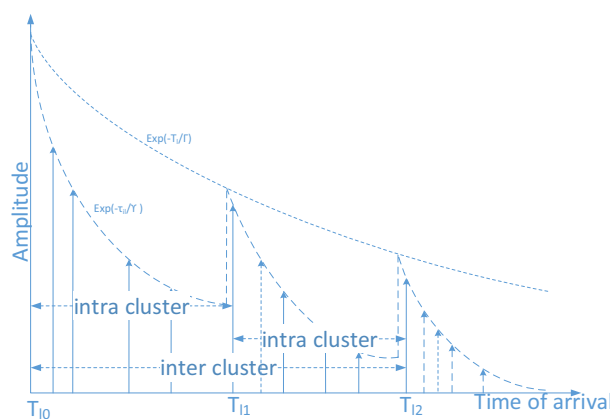


Fig. 3 Saleh-Valenzuela propagation model

where T_l is the arrival time of the l th cluster and τ_{il} is the arrival time of the i th path in the l th cluster. And we set the time constants T_l and τ_{il} or the inter- and intra-cluster as 300 ns and 5 ns, respectively, as Poisson distributions. Γ is a constant of cluster arrival decay time, γ indicates a constant of ray arrival decay time, $\Gamma = 60$ ns and $\gamma = 20$ ns.

3 Problem solving

In the section, roughly estimating the amplitude and TOA based on the subspace projection is introduced, the signal space is reconstructed using the roughly estimated amplitude and TOA, and the high-precision TOA is calculated by the gradient descent method.

3.1 Process of solved

In Fig. 4, the WiFi network collected by the PC contains CSI between sniffers and between the target device and AP. The CIR peak is shifted to the center of the index and filtered. In a short time period, the amplitude is roughly estimated by least squares estimation, and the TOA is roughly estimated by subspace projection. The

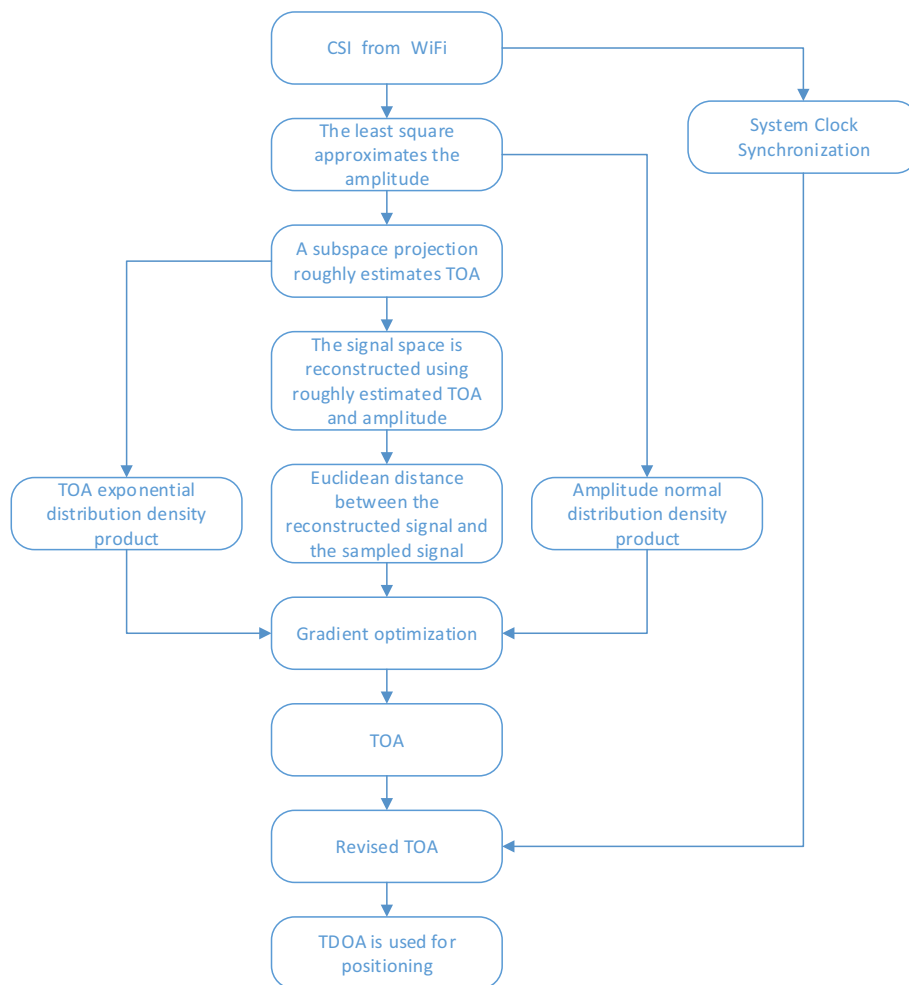


Fig. 4 Algorithm framework is based on CSI localization

roughly estimated amplitude and the TOA can reconstruct the signal space. Through the Euclidian distance between the reconstructed signal space and the sampled signal space and the exponential distribution density product and amplitude normal distribution density product of TOA, the high-precision TOA can be estimated by gradient descent. The timestamps between sniffers are used to estimate the system clock synchronization and clock offset correction of the acquired TOA. Then, weighted mean filtering is used to improve positioning performance further. Finally, TDOA is used to locate the target device online on a PC.

3.2 Subspace projections give rough estimates of TOA and amplitude

In the section, we propose to filter the CIR and shift the peak value to the center of the index, estimate the amplitude by least square, and finally estimate the TOA by subspace projection.

3.2.1 Signal of CSI filter

The sampled TOA signal contains white noise and interference. This information is going to have a significant impact on our TOA estimates. So we need to attenuate and filter out these distracting messages. As shown in Fig. 5, the impulse response is found from the channel estimate by taking the inverse fast Fourier transform (IFFT). The resulting impulse response has samples spaced by 10ns. This oversamples the impulse response somewhat. The impulse response peak on the left can easily be considered the wave peak in the region where the estimated TOA is located, making the algorithm easy to fall into a local optimum. Therefore, we determine the approximate TOA region for positioning by finding the highest peak and then shift the peak signal to the center of the index by using the signal offset method to estimate the TOA, as shown in Fig. 6.

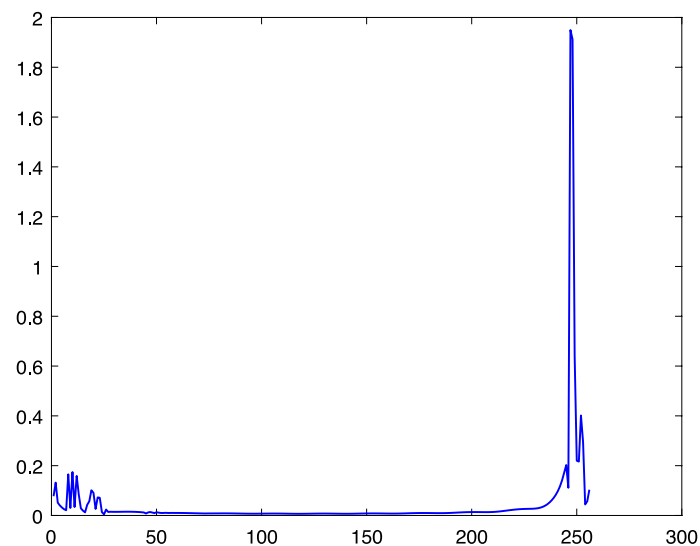


Fig. 5 CSI time-domain raw signal

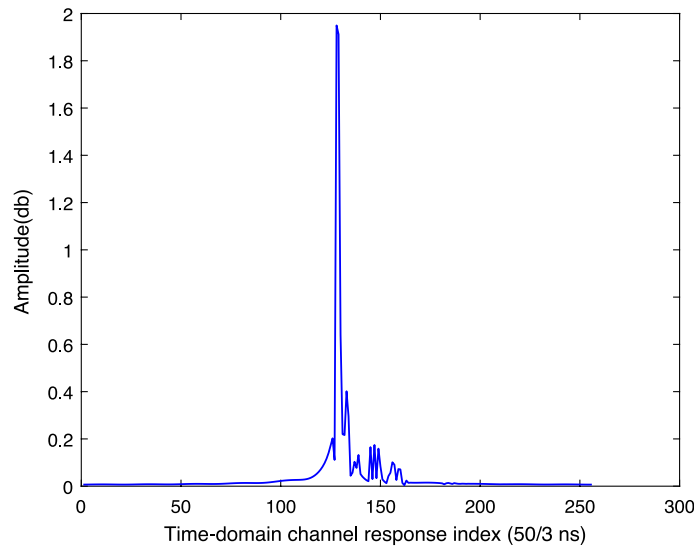


Fig. 6 CSI time-domain shift signal

3.2.2 Least squares amplitude estimation

According to (3) and SVPM, and the CIR sampled from the time-domain CSI [44], there are two random numbers in the model, one is the amplitude obeying Poisson distribution, the other is the diameter of arrival time following an exponential distribution. The existence of two random numbers makes it difficult to estimate TOA. The least squares method is used to obtain the amplitude estimation, thus solving the problem of estimating TOA by the subgradient method and providing important reference data for signal reconstruction.

This paper considers super-resolution TOA estimation based on frequency-domain measurement of the channel response. The sampled CFR from the frequency-domain CSI (2) can also be expressed as [46, 47]:

$$H(f) = \sum_{k=0}^L \alpha_k e^{-j2\pi f \tau_k}, \tag{6}$$

where f denotes frequency bands or bandwidth. The parameters τ_k and α_k are random time-variant functions because of environmental state changes and communication equipment factors. According to the SVPM, τ_k and α_k follow the exponential distribution and Poisson distribution, respectively. L indicates the total number of propagation paths.

In fact, we collected the measurement data are discrete data by sampling channel at equally spaced frequencies, and considering white noise in signal, so the discrete frequency-domain channel response is expressed as:

$$y(k) = H(f_k) + n(k) = \sum_{k=0}^{L-1} \alpha_k e^{-j2\pi(f_0+k\Delta f)\tau_k} + n(k), \tag{7}$$

where $n(i)$ denotes white measurement noise with mean zero. f is the center frequency, and Δf is the k th frequency subband. Then, this signal model in vector form can be written as

$$\mathbf{y} = \mathbf{H} + \mathbf{n} = \mathbf{S}\mathbf{m} + \mathbf{n}, \tag{8}$$

where

$$\begin{aligned} \mathbf{y} &= [y(0) \ y(1) \ \dots \ y(L-1)]^T, \\ \mathbf{H} &= [H(f_0) \ H(f_1) \ \dots \ H(f_{L-1})]^T, \\ \mathbf{n} &= [n(0) \ n(1) \ \dots \ n(L-1)]^T, \\ \mathbf{S} &= [\mathbf{s}(\tau_0) \ \mathbf{s}(\tau_1) \ \dots \ \mathbf{s}(\tau_{L-1})], \\ \mathbf{s}(\tau_k) &= [1 \ e^{-j2\pi(f_0+\Delta f)\tau_k} \ \dots \ e^{-j2\pi(f_0+(L-1)\Delta f)\tau_k}]^T, \\ \mathbf{m} &= [\alpha_0 \ \alpha_1 \ \dots \ \alpha_{L-1}]^T, \end{aligned} \tag{9}$$

where the superscript T expresses the matrix transpose operation.

Because the number of path τ_k is far smaller than the number of CSI sampled. At the same time, in the indoor positioning scene, the amplitude value of the signal transmitted in a short time is a relatively stable value. Therefore, there exists a set of \mathbf{m} , such that

$$\min \sum_{k=0}^L (\mathbf{y} - \mathbf{S}\mathbf{m})^2. \tag{10}$$

So the amplitude value $\hat{\mathbf{m}}$ can be estimated by the least squares estimation, we have

$$\hat{\mathbf{m}} = (\mathbf{S}^H \mathbf{S})^{-1} \mathbf{S}^H \mathbf{y}. \tag{11}$$

3.2.3 Subspace projection TOA estimation

The subspace projection plays an important role in the initial estimated TOA. As shown in Fig. 7, in order to estimate TOA [46], we project the multidimensional vector \mathbf{y} onto the time axis \mathbf{t} , and according to the amplitude value remains constant for a shorter time and formula (11) [48], so we get y'_0 .

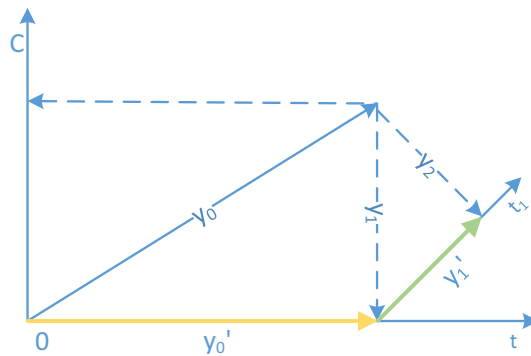


Fig. 7 Projection of \mathbf{y} in \mathbf{t} generated vector

$$\mathbf{y}'_0 = \mathbf{S}(\mathbf{S}^H \mathbf{S})^{-1} \mathbf{S}^H \mathbf{y}_0, \tag{12}$$

where \mathbf{y}_1 is the residual of \mathbf{y}_0 and \mathbf{y}'_0 in Fig. 7, and it can be written as

$$\begin{aligned} \mathbf{y}_1 &= \mathbf{y}_0 - \mathbf{y}'_0, \\ &= \mathbf{y}_0 - \mathbf{S}(\mathbf{S}^H \mathbf{S})^{-1} \mathbf{S}^H \mathbf{y}_0, \\ &= [\mathbf{I} - \mathbf{S}(\mathbf{S}^H \mathbf{S})^{-1} \mathbf{S}^H] \mathbf{y}_0. \end{aligned} \tag{13}$$

Due to the change of \mathbf{y} changing in subspace, when \mathbf{y} is the closest to the time axes \mathbf{t} , the corresponding time τ_k value is TOA. In other words, the inner product of \mathbf{y}_1 should be minimum, at the same time, \mathbf{y}_1 is perpendicular to \mathbf{y}'_0 [49, 50]. So we have

$$\begin{aligned} \min_{\tau_k} \mathbf{y}^H \mathbf{y} &= \min_{\tau_k} \mathbf{y}_{\perp}^H \mathbf{y}, \\ &= \min_{\tau_k} \left(\mathbf{y}^H [\mathbf{I} - \mathbf{S}(\mathbf{S}^H \mathbf{S})^{-1} \mathbf{S}^H] \right. \\ &\quad \left. \times [\mathbf{I} - \mathbf{S}(\mathbf{S}^H \mathbf{S})^{-1} \mathbf{S}^H] \mathbf{y} \right), \\ &= \min_{\tau_k} \left(\mathbf{y}^H \mathbf{y} - \frac{\mathbf{y}^H \mathbf{S} \mathbf{S}^H \mathbf{y}}{\mathbf{S}^H \mathbf{S}} \right), \end{aligned} \tag{14}$$

Since both $\mathbf{y}^H \mathbf{y}$ and $\mathbf{S}^H \mathbf{S}$ are constant [50, 51], the subspace peak search can be written as

$$\mathbf{P}_{subspace} = \mathbf{y}^H \mathbf{S}. \tag{15}$$

Then, τ_k can be estimated as follows:

$$\hat{\tau}_k = \arg \max_{\tau_k} (\mathbf{y}^H \mathbf{S}), \tag{16}$$

where τ_1 is the first arrival time. Obviously, the second arrival time τ_2 is taken when the inner product of \mathbf{y}_2 is the minimum from Fig. 7. So the proposed algorithm can be summarized in Algorithm 1.

Algorithm 1 Subspace find out the arrival times

Require:

- 1: Input the vector of received signals \mathbf{y} and bandwidth \mathbf{f}
- 2: Initialize the time parameter $\tau_{All} \in [1 : 500]$

Ensure: The vector of arrival times τ_k

- 3: **while** Path number **do**
 - 4: Calculate corresponding times frequencies point vector with $\mathbf{P}_{subspace}$ by (15)
 - 5: Calculate the arrival times τ_k when the value of $\mathbf{P}_{subspace}$ is maximum by (16)
 - 6: Calculate residual \mathbf{y}_1 as latest matrix \mathbf{y} by (13)
 - 7: Recode τ_k
 - 8: **end while**
-

3.3 Gradient descent methods to estimate TOA

The TOA estimated by the least squares estimation and subspace projection is based on the principle that the amplitude value is unchanged in a short time, so the estimated TOA still has a significant error, and the noise space is not very good. Still, it provides a reference data reconstruction according to the signal. Therefore, the method improves the operation efficiency of estimating TOA and effectively avoids the gradient descent method into a local optimum. We use the exponential distribution of time and the normal amplitude distribution to get their distribution density. We use the estimated TOA and amplitude to get the Euclidean distance between the sampled frequency-domain signal and the reconstructed frequency-domain signal gradient descent method.

The gradient descent method is a common first-order optimization method, which is one of the simplest and most classical methods for solving unconstrained optimization problems [52]. Based on (6), the signal space $H(f)$ in the frequency domain is reconstructed by using the arrival time obtained by the subspace projection and the amplitude value obtained by the least squares, so we consider an unconstrained optimization problem $\min_f F(f)$

$$\min_f F(f) = H(f) - H_1(f), \tag{17}$$

The domain of $H(f)$ is in $(0, \infty)$, so $H(f)$ is defined in the domain $H(f)$ we would have

$$\begin{aligned} H'(f) &= \lim_{\Delta f \rightarrow 0} \frac{H(f + \Delta f) - H(f)}{\Delta f}, \\ &= \lim_{\Delta f \rightarrow 0} \frac{\sum_{k=0}^L \alpha_k e^{-j2\pi(f+\Delta f)\tau_k} - \sum_{k=0}^L \alpha_k e^{-j2\pi f\tau_k}}{\Delta f}, \\ &= \lim_{\Delta f \rightarrow 0} \frac{\sum_{k=0}^L \alpha_k e^{-j2\pi(\Delta f)\tau_k}}{\Delta f}, \\ &= \lim_{\Delta f \rightarrow 0} \sum_{k=0}^L \alpha_k e^{-j2\pi\tau_k} \frac{e^{j2\pi\tau_k \Delta f} - 1}{\Delta f}, \\ &= \lim_{\Delta f \rightarrow 0} \sum_{k=0}^L \alpha_k e^{-j2\pi\tau_k} e^{j2\pi\tau_k \Delta f} \frac{e^{j2\pi\tau_k \Delta f} - 1}{\Delta f}, \\ &= \lim_{\Delta f \rightarrow 0} \sum_{k=0}^L \alpha_k e^{-j2\pi\tau_k} e^{j2\pi\tau_k \Delta f} \frac{e^{j2\pi\tau_k \Delta f} - 1}{\Delta f}, \\ &= \lim_{\Delta f \rightarrow 0} \sum_{k=0}^L \alpha_k e^{-j2\pi\tau_k} e^{j2\pi\tau_k \Delta f} \frac{e^{j2\pi\tau_k \Delta f} - 1}{\Delta f}, \\ &= \lim_{\Delta f \rightarrow 0} \sum_{k=0}^L \alpha_k e^{-j2\pi\tau_k} e^{j2\pi\tau_k \Delta f} \frac{e^{j2\pi\tau_k \Delta f} - 1}{\Delta f}, \\ &= \lim_{\Delta f \rightarrow 0} \sum_{k=0}^L \alpha_k e^{-j2\pi\tau_k} e^{j2\pi\tau_k \Delta f} \frac{e^{j2\pi\tau_k \Delta f} - 1}{\Delta f}, \end{aligned} \tag{18}$$

where $f \in (0, \infty)$, α_k and τ_k are two constants; for any point f in the interval, there is a derivative that corresponds to it, so $H(f)$ and $F(f)$ are continuous differentiable functions in the domain. If we can construct a sequence $f_0, f_1, f_2, \dots, f_n$ that can be able to satisfy $F(f_{t+1}) \neq F(f_t), t \in (0, n)$, then we can perform the process continuously to converge to the local minimum.

However, in order to obtain the optimal value, we according to the gradient descent of τ and α , changing in the process of using the amplitude of normal distribution and arrival time of exponential distribution characteristic, to obtain the distribution of t and h density product, as a parameter of gradient evaluation, at the same time using the received frequency-domain signals and according to the time and frequency-domain signal amplitude of the Euclidean distance, as the parameters of gradient evaluation.

3.3.1 Exponential distribution of the arrival times

According to the SVPM [44], the TOA follows an exponential distribution, and the probability density function (PDF) of exponential distribution reflects the probability distribution effect TOA. The PDF is consistent with the problem constraints and any prior knowledge and mathematically tractable, so we use the PDF of the TOA as one of the evaluation parameters for gradient optimization. The PDF of the exponential distribution is written as

$$F_{exponent}(\tau; \lambda) = \begin{cases} \lambda e^{-\lambda\tau}, & \text{if } \tau \geq 0; \\ +0, & \text{if } \tau < 0. \end{cases} \tag{19}$$

The arrival times include the intra-cluster and inter-cluster. If we use the delay of the l th cluster, λ is $\frac{1}{\Gamma}$. However, if using the delay of the k th path in the l th cluster, λ is $\frac{1}{\gamma}$. Γ and γ derive from formula (5), where τ is the time corresponding to each paths. Because time is qualitative, τ always is greater than zero. And we calculate is the PDF of exponential distribution of time, which can reflect the probability distribution of time, so it can be expressed as

$$F_{e_density}(\tau_{k=1}; \lambda) = \prod_{k=1}^N \lambda e^{-\lambda\tau_k}, \quad \text{if } \tau_k \geq 0, \tag{20}$$

where N is the total number of paths, k is the number of paths, and F_τ is the exponential distribution density product of all paths. Because the PDF of one of the time exponential distributions F may be zero, this will result in F_τ being zero, thus affecting the reliability of the system. Take $F_{e_density}$ logarithm which can effectively avoid the occurrence of one of the F 0, $F_{e_density}$ also is zero, and it is written as

$$F_{e_J}(\tau_k; \lambda) = \sum_{k=1}^N (\log \lambda - \lambda\tau_k), \quad \text{if } \tau_k \geq 0. \tag{21}$$

3.3.2 Normal distribution density of the amplitude

The amplitude α_k is obtained by the least squares from formula (11). According to the SVPM, it can be known that the amplitude follows the normal distribution [44], and the density of the normal distribution represents the distribution effect of the random variable amplitude α_k , which can be written as

$$F_{normal}(\alpha_k) = \frac{1}{\sigma\sqrt{2\pi}} e^{-\frac{(\alpha_k)^2}{2\sigma^2}}, \tag{22}$$

where we set $\mu = 0$, σ is the standard deviation [44], and k is the number of amplitude,

The product of the amplitude normal distribution density values of each path of the amplitude reflects the normal distribution effect of all the amplitude values, which can be expressed as

$$F_{k_density}(\alpha_k) = \prod_{k=1}^N \frac{1}{\sigma_k \sqrt{2\pi}} e^{-\frac{(\alpha_k)^2}{2\sigma_k^2}}, \tag{23}$$

where k is the number of amplitude, and N is the total number of amplitude. However, since one of F_{normal} may be zero, it takes the logarithm to avoid $F_{n_density} = 0$, thus improving the stability of the system. So it is written as

$$F_{n_l}(\alpha_k) = \sum_{k=1}^N \left(\log \frac{1}{\sigma_k \sqrt{2\pi}} - \frac{(\alpha_k)^2}{2\sigma_k^2} \right). \tag{24}$$

3.3.3 Euclidean distance between received and reconstructed frequency-domain signals

Amplitude α_k is given from formula (11). τ_k is given by subspace methods from formula (16), so the reconstructed frequency-domain channel response Γ can be obtained by (6). Then, the Euclidean distance between the reconstructed frequency-domain channel response Γ and the received frequency-domain channel response H is obtained, and it can be written as

$$D(H, \Gamma) = \sum_{k=1}^N \sqrt{(H_1 - \Gamma_1)^2 + (H_2 - \Gamma_2)^2 + \dots + (H_k - \Gamma_k)^2}, \tag{25}$$

where N is both the number of paths τ_k and amplitude α_k .

With estimation of the arrival time τ , H will also vary. When $D(H, \Gamma)$ is the minimum, τ_k should be the closest to the ground truth arrival times.

3.3.4 Evaluation method

The evaluation of the gradient descent includes the probability density of exponential distribution, the probability density of normal distribution and Euclidean distance. Larger PDF values for both exponential and normal distributions indicate that the estimated arrival time τ corresponds better to the exponential distribution, and the amplitude α corresponds better to the normal distribution. The smaller the calculated Euclidean distance is, the closer the calculated arrival time τ and amplitude α are to the true values. Therefore, the evaluation of the gradient method is expressed as

$$P(\tau | \lambda, \alpha, H, \Gamma) = \frac{1}{F_{e_l}(\tau, \lambda) + F_{n_l}(\alpha)} + D(H, \Gamma). \tag{26}$$

3.4 The system clock synchronization

In the WiFi-WASP, each sniffer in the system has a local clock, and they are not synchronized with each other, which makes it difficult to locate. Therefore, system clock synchronization is an important problem to solve in location estimation. In order to solve the clock synchronization problem in the process of system positioning, the sniffer clock needs to be

post-synchronized by estimating and compensating the clock tilt and clock offset, so as to estimate the packet arrival time according to a common reference clock. The location of the sniffer and the location of the target are expressed as $s_j = [x_j, y_j, z_j]^T$ ($j = 1, \dots, J$) and $\Gamma = [x, y, z]^T$, where J is the number of sniffers. Assuming that the target device transmits the packet at Γ and at time t_{Tx} , the arrival time r_j of the corresponding radio signal measured by any sniffer is

$$r_j = (1 + \alpha_j) \left(t_T + \frac{d_{j\Gamma}}{c} + \beta_j + \Delta t_j + e_j \right), j = 1, \dots, J, \tag{27}$$

where α_j and β_j represent the clock skews and clock offsets of sniffer j , respectively. $d_{j\Gamma} \triangleq |s_j - \Gamma|$ represents the true distance between the target device and sniffer j , c is the speed of light, Δt_j is the hardware delay (e.g., the delay caused by radio frequency (RF) circuits), and e_j is the time measurement error. In the process of system operation, in order to avoid clock drift, set the values of α and Δt to be very small, Eq. (27) can be rewritten as

$$r_j = \Delta t_j + (1 + \alpha_j) \left(t_{Tx} + \frac{d_j}{c} + \beta_j + e_j \right), j = 1, \dots, J, \tag{28}$$

In a short period of time (less than 0.5 s), the synchronous arrival time measurement of sniffer j t_{Tj} can be expressed as

$$t_{Tj} = \frac{r_j - \Delta t_j}{1 + \alpha_j} - \beta_j - e_j, \tag{29}$$

Assume that the WiFi-WASP device sends two consecutive packets at t_n and t_{n+1} , respectively, with a time interval of less than 0.5 s. The time values received by different sniffers are denoted by r_j^n and r_k^n , respectively. Therefore, the difference between the clock skews of different sniffers can be approximated as

$$\alpha_j - \alpha_k \approx \frac{r_j^{n+1} - r_j^n}{r_k^{n+1} - r_k^n} - 1, \tag{30}$$

where j and k are different sniffers. Using (31) to estimate the clock skews of the sniffer k by specifying one of the sniffers as a reference clock (i.e., $\alpha_j = 0$), it can be expressed as

$$\alpha_k \approx \frac{r_j^{n+1} - r_j^n}{r_k^{n+1} - r_k^n} - 1. \tag{31}$$

Since the location of the sniffer is known, it is easy to measure the true distance between the transmitter and the sniffer. Using formula (27), the clock offset between different sniffers can be written approximately

$$\beta_j - \beta_k \approx \frac{r_j}{1 + \hat{\alpha}_j} - \frac{r_k}{1 + \hat{\alpha}_k} - \frac{d_j}{c} + \frac{d_k}{c}. \tag{32}$$

$\hat{\alpha}_j$ and $\hat{\alpha}_k$, respectively through (31) estimate the clock skew of the j th and k th sniffer. β_j and β_k indicate the clock offset of the j th and k th sniffer, respectively. Using (33)

to estimate the clock offset of the sniffer k by specifying one of the sniffers as a reference clock (i.e., $\beta_k = 0$), it can be expressed as

$$\beta_j \approx \frac{r_j}{1 + \hat{\alpha}_j} - \frac{r_k}{1 + \hat{\alpha}_k} - \frac{d_j}{c} + \frac{d_k}{c}. \tag{33}$$

The estimated clock skews and clock offsets are used to correct the measured arrival time delay of data packets. Meanwhile, the time delay after system clock synchronization is estimated using the reference clock of the sniffer.

3.5 TDOA method

Based on WiFi-WASP system, the measurement error of the direct path of signal propagation outdoors obeys Gaussian distribution, while the measurement error of signal propagation indoors does not. Therefore, Taylor algorithm of TDOA is used to locate the target device. Taylor algorithm A recursive form of hyperbolic equation solving algorithm. In order to ensure the convergence of the algorithm, the initial position deviation should not be too large. There are J sniffers involved in locating the target device, and the position of the j th sniffer is $s_j = (x_j, y_j)^T$, and the position coordinate of the target device is $\Gamma = (x, y)^T$.

The distance between the target device and the k th sniffer is expressed as

$$r_j = \sqrt{(x_j - x)^2 + (y_j - y)^2} \tag{34}$$

The distance difference $r_{j,1}$ between the target device and the sniffer j and 1 can be expressed as

$$r_{j,1} = \sqrt{(x_j - x)^2 + (y_j - y)^2} - \sqrt{(x_1 - x)^2 + (y_1 - y)^2} \tag{35}$$

The first step is to give an initial estimate of the location of the target device $u_0 = (x_0, y_0)^T$, which can be obtained by the weighted least square method. For (35) at the initial estimation position, the first-order Taylor series expansion can be obtained

$$\eta = h - G\delta \tag{36}$$

where η represents residuals and $\delta = (\Delta x, \Delta y)^T$ represents the error vector estimated for the unknown position of the target device and

$$h = \begin{bmatrix} r_{2,1} - (r_2 - r_1) \\ r_{2,1} - (r_2 - r_1) \\ \dots \\ r_{M,1} - (r_M - r_1) \end{bmatrix} \tag{37}$$

$$G = \begin{bmatrix} \frac{x_1 - x_0}{r_1} & -\frac{x_2 - x_0}{r_2} & \frac{y_1 - x_0}{r_1} & -\frac{y_2 - x_0}{r_2} \\ \frac{x_1 - x_0}{r_1} & -\frac{x_3 - x_0}{r_3} & \frac{y_1 - x_0}{r_1} & -\frac{y_3 - x_0}{r_3} \\ \dots & \dots & \dots & \dots \\ \frac{x_1 - x_0}{r_1} & -\frac{x_M - x_0}{r_M} & \frac{y_1 - x_0}{r_1} & -\frac{y_M - x_0}{r_M} \end{bmatrix} \tag{38}$$

The weighted least squares solution of formula (36) is

$$\delta = (\Delta x, \Delta y)^T = (G^T Q^{-1} G)^{-1} G^T Q^{-1} h \quad (39)$$

where Q represents the covariance matrix of the measured values of TDOA, and the initial value of the next iteration can be obtained through formula (39)

$$x'_0 = x_0 + \Delta x, y'_0 = y_0 + \Delta y. \quad (40)$$

Plug this value into the next iteration, and the general ε threshold takes 10^{-3} until it recurs to

$$|\Delta x| + |\Delta y| < \varepsilon. \quad (41)$$

At this point, we can get the coordinate estimate value of the target device to be tested (x'_0, y'_0) .

4 Experimental results

The system performance was evaluated under outdoor line-of-sight (LOS) conditions and indoor conditions. During each experiment, an 802.11ac wireless local area network was set up, which operates in channel 149 with 80 MHz bandwidth. A laptop with a WiFi USB dongle is used as the target device and regularly pings the AP to generate WiFi traffic. The packets transmitted by the APs were used for synchronizing the sniffers.

4.1 Outdoor test

The system was tested under outdoor line-of-sight (LOS) conditions to evaluate its performance. We deployed six sniffers around a WiFi network for the outdoor LOS tests with one access point and one WiFi dongle. The topology of the system is shown in Fig. 8. The size of the experimental area was 900 m². The target moved across the test area. Figure 5 shows the positioning results for the outdoor test. It can be seen that the positioning results are consistent with the actual locations.

Figure 9 shows the positioning accuracy of our system when the TOA is estimated using the subspace and gradient descent (SGD) and MUSIC and ESPRIT algorithm. It can be seen that the 80 percentile positioning error is 0.75 m, and 1 m in 90% with the SGD. Compared with MUSIC and ESPRIT's TOA estimation methods, the accuracy of SGD's TOA estimation method is much higher.

4.2 Indoor test

The indoor experiment is shown in Fig. 10. With the same conditions as the outdoor experiment, we deployed six sniffers in the assembly hall, covering an area of around 700 m². One standard WiFi device was placed at known locations for synchronizing the sniffer clocks. The target was to collect data from 17 locations in the assembly hall. Figure 11 shows the target position and estimated position. It can be seen that except for the poor reflection effect of the seat in the Y-axis direction, the estimated position is consistent with the actual position, which can meet the needs of many indoor positioning.

Figure 12 shows the positioning effect of our system when using SGD, MUSIC and ESPRIT algorithms to estimate TOA. It can be seen that the about 48 percentile positioning error is 0.5 m and 1 m in 74%. Compared with MUSIC and ESPRIT's

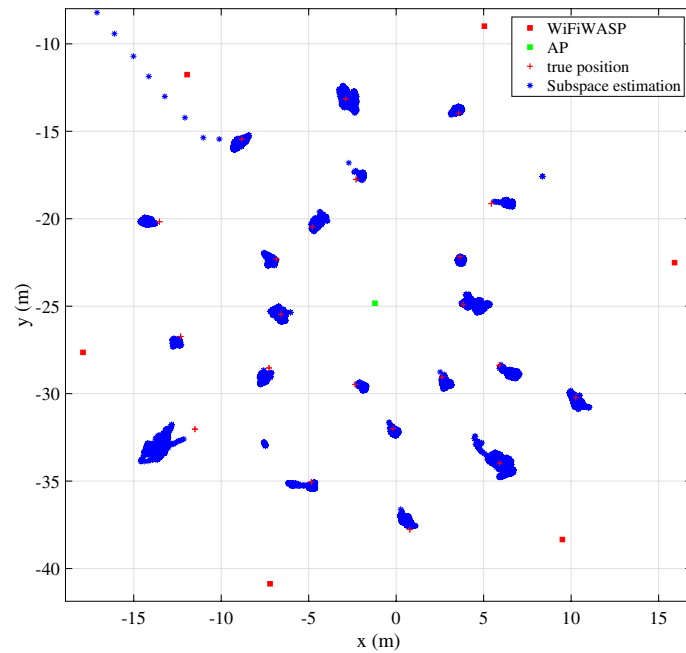


Fig. 8 Positioning results in outdoor LOS environments

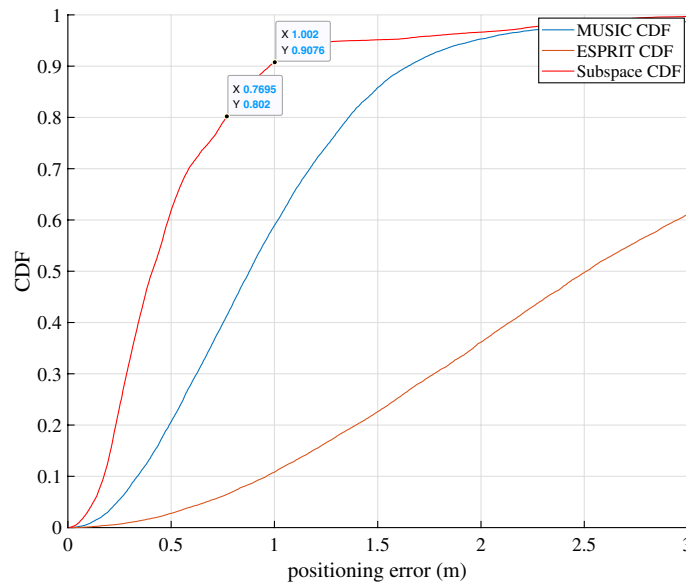


Fig. 9 Cumulative distribution function of the positioning errors for the outdoor LOS test

TOA estimation method, SGD's TOA estimation method has higher accuracy. Under similar conditions, the SpotFi is the method proposed in [31], M. Kotaru et al. has a positioning error of 0.5 m with less than 40%, and the 60 percentile positioning error is 1 m.



Fig. 10 Estimated target locations in the indoor environment data collection

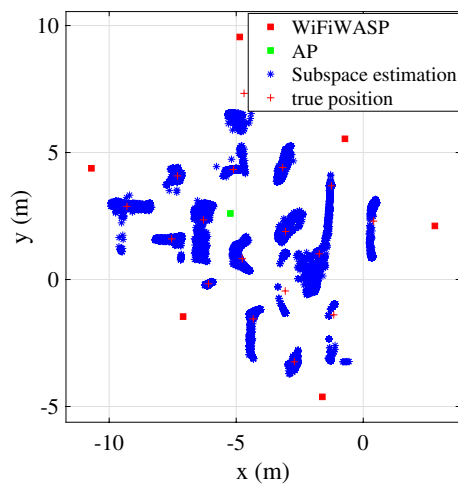


Fig. 11 Estimated target locations in the indoor experiment

5 Conclusion

With the increasing demand for positioning, the existing positioning methods are challenging to meet the convenience of deploying equipment without satellite positioning. The proposed method for estimating TOA is expected to better adapt to the business needs of device deployment. In this paper, a rough estimation of amplitude based on least squares and a rough estimation of TOA based on subspace projection is designed. The signal space is reconstructed using the estimated amplitude and TOA, which reduces the complexity of the calculation. The normal distribution of amplitude, the exponential distribution of TOA and the Euclidean distance between the reconstructed signal and the sampled signal are used to improve the positioning accuracy. The proposed algorithms were validated experimentally on an outdoor localization system deployed with six anchors covering 900 m². The results show that

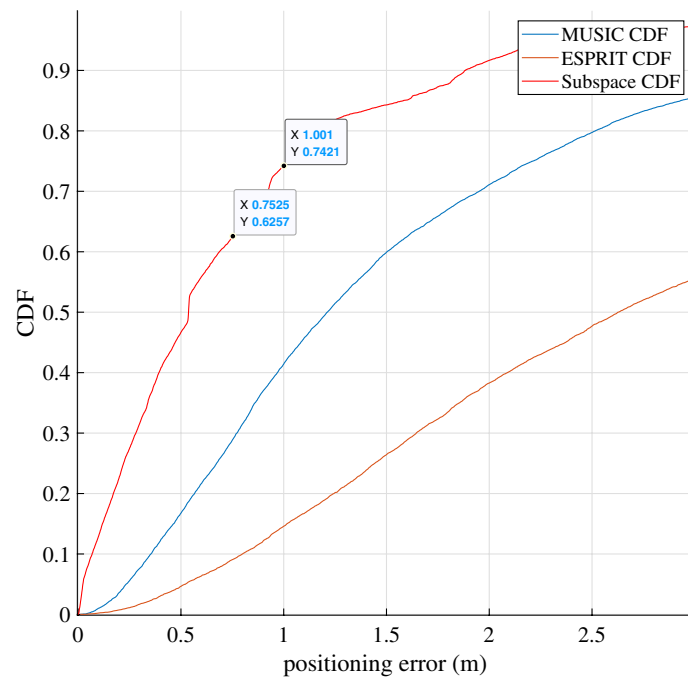


Fig. 12 Cumulative distribution function of the positioning errors for the indoor test

the proposed algorithm has high precision. At the same time, it has been verified that the positioning effect is better indoors. Compared with the fingerprint positioning method, the positioning method adopted in this paper has the advantage of not needing to sample data in the positioning environment in advance, so it has a broad application prospect.

Acknowledgements

Acknowledgments are not compulsory. Where included they should be brief. Grant or contribution numbers may be acknowledged. Please refer to Journal-level guidance for any specific requirements.

Author contributions

In this work, the first, third and fifth authors put forward the overall research idea. The first and third authors completed the virtual simulation experiment and data collection. The second and fourth authors provide data management, validation, funding support and guidance on research ideas. The first author wrote the manuscript, and the third, fifth, sixth and seventh authors provided the methodology, writing review and revised the manuscript. All authors read and approved the final manuscript.

Funding

This work is supported by the National Key Research and Development Program of China with Grant Nos. 2018YFB0505202, and XJZK201802, and supported by the Science and Technology Research Program of Chongqing Municipal Education Commission with Grant No. KJQN202003407. The Research Project of Shanghai Polytechnic University No.EDG21QD15, and supported by the Science and Technology Major Program of Fujian Province (No. 2022HZ026007)

Availability of data and materials

As the data came from a third-party department, CSIRO, which was not authorized to release the data, is not applicable.

Declarations

Ethics approval and consent to participate

This research does not use animals or humans to make research on them. It is just a computer simulation program.

Competing interests

The authors declare that they have no competing interests to report regarding the present study.

Received: 8 October 2022 Accepted: 5 September 2023

Published online: 06 November 2023

References

- H. Liu, H. Darabi, P. Banerjee, J. Liu, Survey of wireless indoor positioning techniques and systems. *IEEE Trans. Syst. Man Cybern. Part C (Appl. Rev.)* **37**(6), 1067–1080 (2007). <https://doi.org/10.1109/TSMCC.2007.905750>
- M. Hedley, J. Zhang, Accurate wireless localization in sports. *Computer* **45**(10), 64–70 (2012). <https://doi.org/10.1109/MC.2012.119>
- Y. Gu, F. Ren, Energy-efficient indoor localization of smart hand-held devices using bluetooth. *IEEE Access* **3**, 1450–1461 (2015). <https://doi.org/10.1109/ACCESS.2015.2441694>
- Y. Gu, F. Ren, Energy-efficient indoor localization of smart hand-held devices using bluetooth. *IEEE Access* **3**, 1450–1461 (2015). <https://doi.org/10.1109/ACCESS.2015.2441694>
- P. Bahl, V.N. Padmanabhan, Radar: an in-building rf-based user location and tracking system. vol 2 (2000), pp. 775–7842. <https://doi.org/10.1109/INFCOM.2000.832252>
- Z. Zhou, L. Shangguan, X. Zheng, L. Yang, Y. Liu, Design and implementation of an RFID-based customer shopping behavior mining system. *IEEE/ACM Trans. Netw.* **25**(4), 2405–2418 (2017). <https://doi.org/10.1109/TNET.2017.2689063>
- B. Kempke, P. Pannuto, P. Dutta, Surepoint: exploiting ultra wideband flooding and diversity to provide robust, scalable, high-fidelity indoor localization: demo abstract (2016). <https://doi.org/10.1145/2994551.2996541>
- Y. Shu, C. Bo, G. Shen, C. Zhao, L. Li, F. Zhao, Magicol: indoor localization using pervasive magnetic field and opportunistic WiFi sensing. *IEEE J. Sel. Areas Commun.* **33**(7), 1443–1457 (2015). <https://doi.org/10.1109/JSAC.2015.2430274>
- P.H. Pathak, X. Feng, P. Hu, P. Mohapatra, Visible light communication, networking, and sensing: a survey, potential and challenges. *IEEE Commun. Surv. Tutor.* **17**(4), 2047–2077 (2015). <https://doi.org/10.1109/COMST.2015.2476474>
- D. Hauschildt, N. Kirchhof, Advances in thermal infrared localization: challenges and solutions (2010), pp. 1–8. <https://doi.org/10.1109/IPIN.2010.5647415>
- J.N. Moutinho, R.E. Araújo, D. Freitas, Indoor localization with audible sound—towards practical implementation. *Pervasive Mob. Comput.* **29**(C), 1–6 (2016). <https://doi.org/10.1016/j.pmcj.2015.10.016>
- C. Yang, H.R. Shao, Wifi-based indoor positioning. *IEEE Commun. Mag.* **53**(3), 150–157 (2015). <https://doi.org/10.1109/MCOM.2015.7060497>
- S. He, S.-H.G. Chan, Wi-fi fingerprint-based indoor positioning: recent advances and comparisons. *IEEE Commun. Surv. Tutor.* **18**(1), 466–490 (2016). <https://doi.org/10.1109/COMST.2015.2464084>
- Y. Ma, G. Zhou, S. Wang, Wifi sensing with channel state information: a survey. *ACM Comput. Surv.* **52**(3), 1–36 (2019). <https://doi.org/10.1145/3310194>
- Z. Yang, Z. Zhou, Y. Liu, From RSSI to CSI: indoor localization via channel response. *ACM Comput. Surv.* **46**(2), 1–32 (2013). <https://doi.org/10.1145/2543581.2543592>
- P. Bahl, V.N. Padmanabhan, Radar: an in-building rf-based user location and tracking system, vol 2 (2000), pp. 775–7842. <https://doi.org/10.1109/INFCOM.2000.832252>
- Y. Gu, Y. Chen, J. Liu, X. Jiang, Semi-supervised deep extreme learning machine for Wi-Fi based localization. *Neuro-computing* **166**(C), 282–293 (2015). <https://doi.org/10.1016/j.neucom.2015.04.011>
- S.-H. Fang, C.-H. Wang, A novel fused positioning feature for handling heterogeneous hardware problem. *IEEE Trans. Commun.* **63**(7), 2713–2723 (2015). <https://doi.org/10.1109/TCOMM.2015.2442989>
- S.-H. Fang, T.-N. Lin, Projection-based location system via multiple discriminant analysis in wireless local area networks. *IEEE Trans. Veh. Technol.* **58**(9), 5009–5019 (2009). <https://doi.org/10.1109/TVT.2009.2025134>
- Z.-A. Deng, Y. Xu, L. Chen, Localized local fisher discriminant analysis for indoor positioning in wireless local area network (2013), pp. 4795–4799. <https://doi.org/10.1109/WCNC.2013.6555352>
- H. Chen, Y. Zhang, W. Li, X. Tao, P. Zhang, Confi: Convolutional neural networks based indoor Wi-Fi localization using channel state information. *IEEE Access* **5**, 18066–18074 (2017). <https://doi.org/10.1109/ACCESS.2017.2749516>
- X. Zhu, W. Qu, X. Zhou, L. Zhao, Z. Ning, T. Qiu, Intelligent fingerprint-based localization scheme using CSI images for internet of things. *IEEE Trans. Netw. Sci. Eng.* **9**(4), 2378–2391 (2022). <https://doi.org/10.1109/TNSE.2022.3163358>
- W. Wei, J. Yan, X. Wu, C. Wang, G. Zhang, A data preprocessing method for deep learning-based device-free localization. *IEEE Commun. Lett.* **25**(12), 3868–3872 (2021). <https://doi.org/10.1109/LCOMM.2021.3116150>
- X. Wang, S. Mao, Deep convolutional neural networks for indoor localization with CSI images. *IEEE Trans. Netw. Sci. Eng.* **7**(1), 316–327 (2020). <https://doi.org/10.1109/TNSE.2018.2871165>
- L. Chen, I. Ahriz, D. Le Ruyet, CSI-based probabilistic indoor position determination: an entropy solution. *IEEE Access* **7**, 170048–170061 (2019). <https://doi.org/10.1109/ACCESS.2019.2955747>
- Y. Jing, J. Hao, P. Li, Learning spatiotemporal features of CSI for indoor localization with dual-stream 3D convolutional neural networks. *IEEE Access* **7**, 147571–147585 (2019). <https://doi.org/10.1109/ACCESS.2019.2946870>
- T.F. Sanam, H. Godrich, A multi-view discriminant learning approach for indoor localization using amplitude and phase features of CSI. *IEEE Access* **8**, 59947–59959 (2020). <https://doi.org/10.1109/ACCESS.2020.2982277>
- X. Dang, X. Si, Z. Hao, Y. Huang, A novel passive indoor localization method by fusion CSI amplitude and phase information. *Sensors* **19**(4), 875 (2019). <https://doi.org/10.3390/s19040875>
- Z. Li, D.B. Acuña, Z. Zhao, J.L. Carrera, T. Braun, Fine-grained indoor tracking by fusing inertial sensor and physical layer information in WLANs (2016), pp. 1–7. <https://doi.org/10.1109/ICC.2016.7511162>

30. M. Kotaru, K. Joshi, D. Bharadia, S. Katti, Spotfi: decimeter level localization using wifi (2015). <https://doi.org/10.1145/2785956.2787487>
31. C. Yang, H.R. Shao, WiFi-based indoor positioning. *IEEE Commun. Mag.* **53**(3), 150–157 (2015). <https://doi.org/10.1109/MCOM.2015.7060497>
32. R. Schmidt, Multiple emitter location and signal parameter estimation. *IEEE Trans. Antennas Propag.* **34**(3), 276–280 (1986). <https://doi.org/10.1109/TAP.1986.1143830>
33. J. Xiong, K. Jamieson, Arraytrack: a fine-grained indoor location system (2013), pp. 71–84
34. M. Hedley, J. Zhang, Accurate wireless localization in sports. *Computer* **45**(10), 64–70 (2012). <https://doi.org/10.1109/MC.2012.119>
35. T. Sathyan, D. Humphrey, M. Hedley, Wasp: a system and algorithms for accurate radio localization using low-cost hardware. *EEE Trans. Syst. Man Cybern. Part C (Appl. Rev.)* **41**(2), 211–222 (2011). <https://doi.org/10.1109/TSMCC.2010.2051027>
36. S. Li, M. Hedley, I.B. Collings, New efficient indoor cooperative localization algorithm with empirical ranging error model. *IEEE J. Sel. Areas Commun.* **33**(7), 1407–1417 (2015). <https://doi.org/10.1109/JSAC.2015.2430273>
37. S. Li, M. Hedley, I.B. Collings, D. Humphrey, TDOA-based localization for semi-static targets in NLOS environments. *IEEE Wirel. Commun. Lett.* **4**(5), 513–516 (2015). <https://doi.org/10.1109/LWC.2015.2449306>
38. S. Li, M. Hedley, K. Bengston, M. Johnson, D. Humphrey, A. Kajan, N. Bhaskar, TDOA-based passive localization of standard WiFi devices (2018), pp. 1–5. <https://doi.org/10.1109/UPINLBS.2018.8559705>
39. P. Cheng, Z. Chen, F. Hoog, C.K. Sung, Sparse blind carrier-frequency offset estimation for OFDMA uplink. *IEEE Trans. Commun.* **64**(12), 5254–5265 (2016). <https://doi.org/10.1109/TCOMM.2016.2615106>
40. H. Ye, G.Y. Li, B.-H. Juang, Power of deep learning for channel estimation and signal detection in OFDM systems. *IEEE Wirel. Commun. Lett.* **7**(1), 114–117 (2018). <https://doi.org/10.1109/LWC.2017.2757490>
41. G. Wang, A. Abbasi, H. Liu, Dynamic phase calibration method for CSI-based indoor positioning (2021), pp. 0108–0113. <https://doi.org/10.1109/CCWC51732.2021.9376003>
42. X. Wang, L. Gao, S. Mao, S. Pandey, CSI-based fingerprinting for indoor localization: a deep learning approach. *IEEE Trans. Veh. Technol.* **66**(1), 763–776 (2017). <https://doi.org/10.1109/TVT.2016.2545523>
43. Z. Zhou, C. Wu, Z. Yang, Y. Liu, Sensorless sensing with WiFi. *Tsinghua Sci. Technol.* **20**(1), 1–6 (2015). <https://doi.org/10.1109/TST.2015.7040509>
44. D. Humphrey, M. Hedley, Prior models for indoor super-resolution time of arrival estimation (2009), pp. 1–5. <https://doi.org/10.1109/VETECS.2009.5073817>
45. K. Pahlavan, A. Levesque, *Wireless Information Networks*, 2nd edn. (Wiley, New York, 2005)
46. C. Zhang, Y. Wang, An improved subspace projection method of underdetermined direction of arrival estimation for frequency hopping signals (2017), pp. 1–2. <https://doi.org/10.23919/ROPACES.2017.7916386>
47. X. Li, K. Pahlavan, Super-resolution toa estimation with diversity for indoor geolocation. *IEEE Trans. Wirel. Commun.* **3**(1), 224–234 (2004). <https://doi.org/10.1109/TWC.2003.819035>
48. D. Humphrey, M. Hedley, Prior models for indoor super-resolution time of arrival estimation (2009), pp. 1–5. <https://doi.org/10.1109/VETECS.2009.5073817>
49. R. Zeng, H. Huang, L. Yang, Z. Zhang, Joint estimation of frequency offset and doppler shift in high mobility environments based on orthogonal angle domain subspace projection. *IEEE Trans. Veh. Technol.* **67**(3), 2254–2266 (2018). <https://doi.org/10.1109/TVT.2017.2766887>
50. H. Hui, Z. Juan, X. Xiong, Z. Linrang, Moving false-targets jamming suppression method for radar based on frequency subspace (2016), pp. 1–4. <https://doi.org/10.1109/RADAR.2016.8059360>
51. L. Huang, Y. Wu, H.C. So, Y. Zhang, L. Huang, Multidimensional sinusoidal frequency estimation using subspace and projection separation approaches. *IEEE Trans. Signal Process.* **60**(10), 5536–5543 (2012). <https://doi.org/10.1109/TSP.2012.2206590>
52. K.U. Sooraj, W.W. Godfrey, Power allocation in OFDM-CR using accelerated gradient descent algorithm (2015), pp. 562–565. <https://doi.org/10.1109/CICN.2015.115>

Publisher's Note

Springer Nature remains neutral with regard to jurisdictional claims in published maps and institutional affiliations.

Submit your manuscript to a SpringerOpen[®] journal and benefit from:

- Convenient online submission
- Rigorous peer review
- Open access: articles freely available online
- High visibility within the field
- Retaining the copyright to your article

Submit your next manuscript at ► [springeropen.com](https://www.springeropen.com)
